Ph.D. Thesis

Universitat de Barcelona
Departament de Geodinàmica i Geofísica

A Magnetotelluric Investigation of Geoelectrical Dimensionality and Study of the Central Betic Crustal Structure

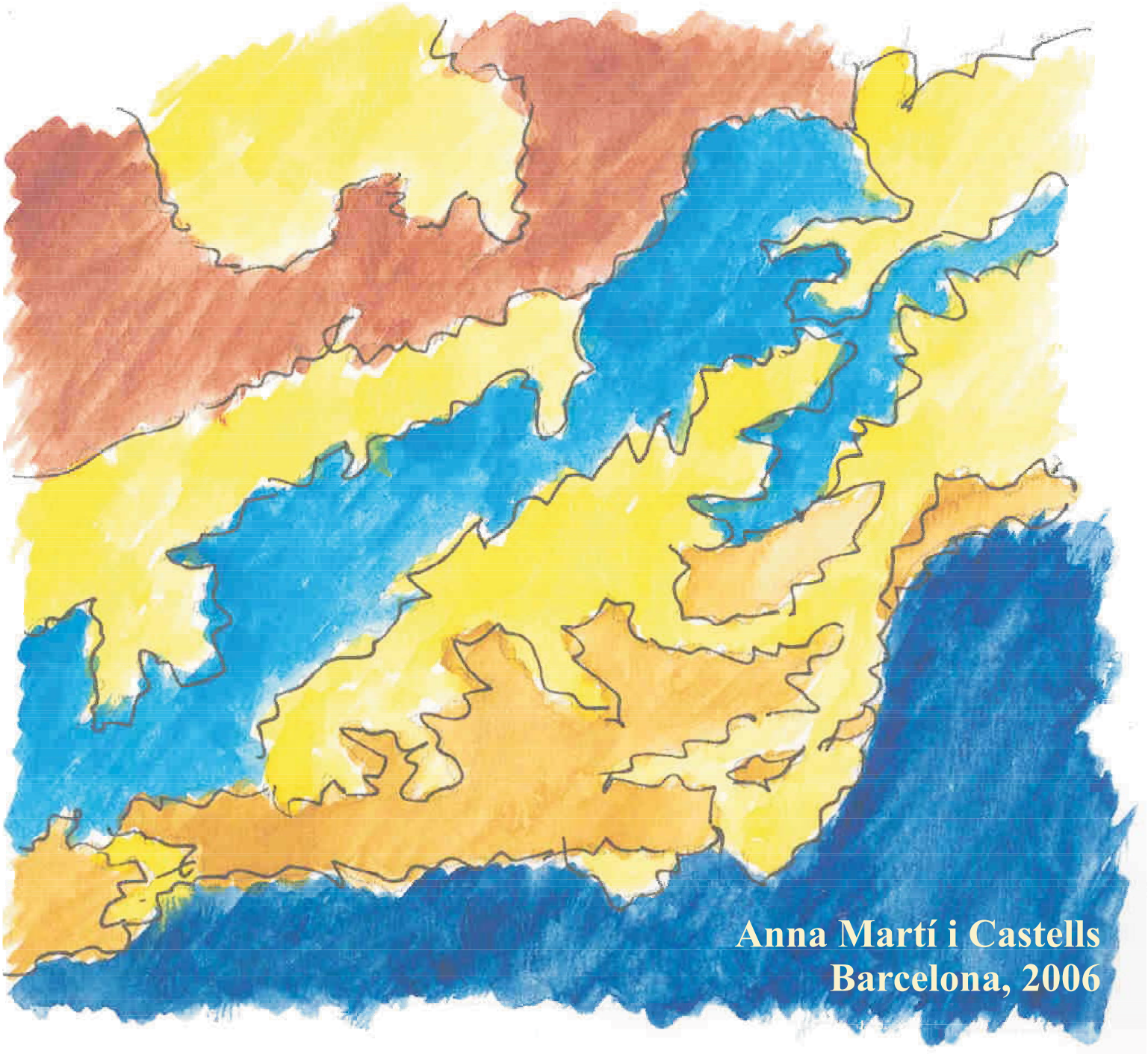

Anna Martí i Castells

Barcelona, 2006

Part I. Introduction to the Magnetotelluric Method

1. The Magnetotelluric Method
2. Geoelectric Dimensionality and Rotational Invariants of the Magnetotelluric Tensor

Chapter 1: The Magnetotelluric Method

This chapter presents the generalities on the magnetotelluric method. It is a description of the basis of the method and its ruling equations, how it is applied and the problems that must be overcome to succeed at doing so. Special care has been taken in describing its current research status and its latest developments.

1.1 Introduction

The magnetotelluric method or magnetotellurics (MT) is an electromagnetic geophysical exploration technique that images the electrical properties (distribution) of the Earth.

The source of energy in the magnetotelluric method is the natural electromagnetic field. When this external energy, known as the primary electromagnetic field, reaches the Earth's surface, part of it is reflected, whereas the remainder penetrates into the Earth, which acts as a conductor, inducing an electric field (known as telluric currents) that at the same time produces a secondary magnetic field.

Magnetotellurics is based on the simultaneous measurement of the total electromagnetic field time variations at the Earth's surface ($\vec{E}(t)$ and $\vec{B}(t)$).

The electrical properties (e.g. electrical conductivity) of the underlying materials can be determined from the relationship between the components of the measured electric and

magnetic field variations, or transfer functions. These are the horizontal electric (E_x and E_y) and the horizontal (B_x, B_y) and vertical (B_z) magnetic components.

According to the behaviour of electromagnetic waves in conductors, the penetration of an electromagnetic wave depends on the oscillation frequency. Hence, the frequency of the electromagnetic fields being measured determines the study depth.

The origins of MT are attributed to Tikhonov (1950) and Cagniard (1953), who established the theoretical basis of the method. In half a century, important developments in formulation, instrumentation and interpretation techniques have yielded MT to be a competitive geophysical method, suitable to image a broad range of geological targets. A review of its historical evolution can be found in Dupis (1997).

1.2 Governing Equations

The electromagnetic fields within a material in a non-accelerated reference frame can be completely described by Maxwell's equations. These can be expressed in differential form and with the International System of Units (SI) as:

$$\vec{\nabla} \times \vec{E} = -\frac{\partial \vec{B}}{\partial t}, \qquad \text{Faraday's law} \qquad (1.1a)$$

$$\vec{\nabla} \times \vec{H} = \vec{j} + \frac{\partial \vec{D}}{\partial t}, \qquad \text{Ampere's law} \qquad (1.1b)$$

$$\vec{\nabla} \cdot \vec{D} = \rho_V, \qquad \text{Gauss's law} \qquad (1.1c)$$

$$\vec{\nabla} \cdot \vec{B} = 0, \qquad \text{Gauss's law for magnetism} \qquad (1.1d)$$

where $\vec{E}$ (V/m) and $\vec{H}$ (A/m) are the electric and magnetic fields, $\vec{B}$ (T) is the magnetic induction, $\vec{D}$ (C/m^2) is the electric displacement and ρ_V (C/m^3) is the electric charge density owing to free charges. $\vec{j}$ and $\partial \vec{D} / \partial t$ (A/m^2) are the current density and the displacement current respectively.

The vectorial magnitudes in Maxwell's equations can be related through their constitutive relationships:

$$\vec{j} = \sigma \vec{E}, \qquad (1.2a)$$

$$\vec{D} = \varepsilon \vec{E}, \qquad (1.2b)$$

$$\vec{B} = \mu \vec{H}. \qquad (1.2c)$$

σ, ε and μ describe intrinsic properties of the materials through which the electromagnetic fields propagate. σ (S/m) is the electrical conductivity (its reciprocal being the electrical resistivity $\rho = 1/\sigma$ (Ω·m)), ε (F/m) is the dielectric permittivity and μ (H/m) is the magnetic permeability. These magnitudes are scalar quantities in isotropic media. In anisotropic materials they must be expressed in a tensorial form. In this work, it will be assumed that the properties of the materials are isotropic.

The electrical conductivity of Earth materials has a wide variation (up to ten orders of magnitude) (Figure 1.1) and is sensitive to small changes in minor constituents of the rock. Since conductivity of most rock matrices is very low (10^{-5} S/m), the conductivity of the rock unit depends in general on the interconnectivity of minor constituents (by way of fluids or partial melting) or on the presence of highly conducting minerals such as graphite (Jones, 1992).

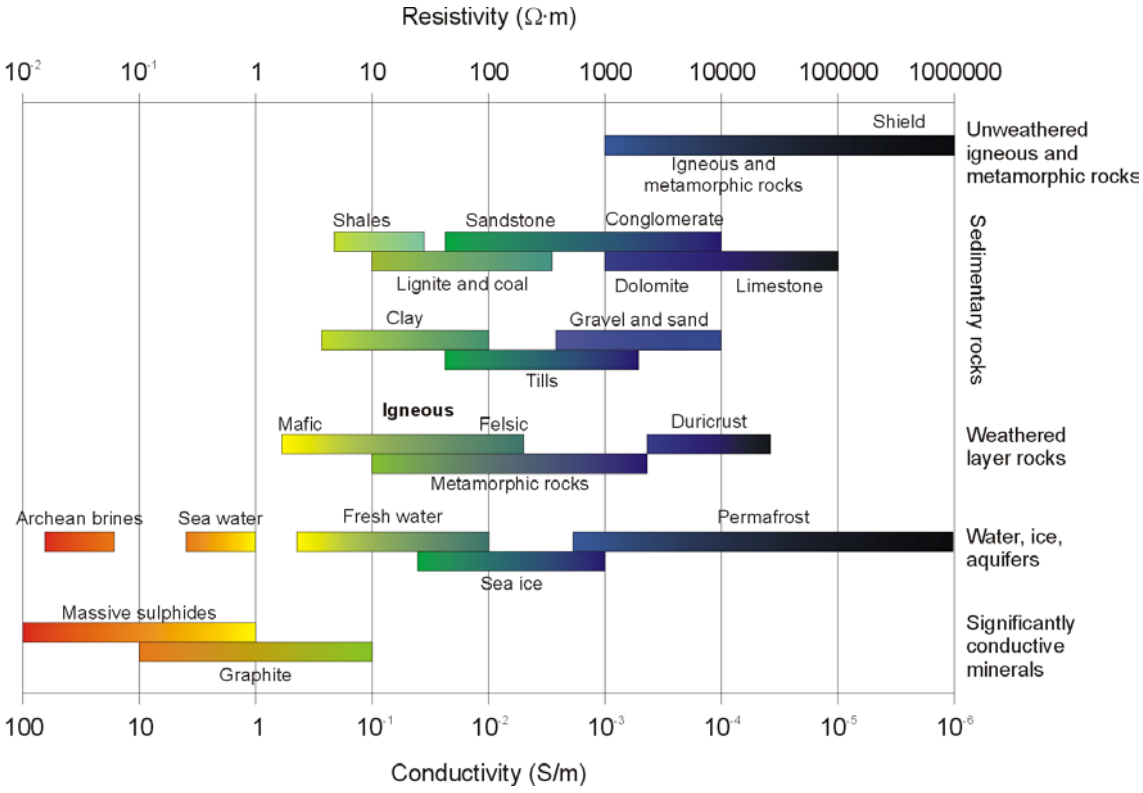

Figure 1.1: Electrical conductivity of Earth materials (modified from Palacky, 1987).

In a vacuum, the dielectric permittivity is $\varepsilon = \varepsilon_0 = 8.85 \cdot 10^{-12}$ F/m. Within the Earth, this value ranges from ε_0 (vacuum and air) to $80\varepsilon_0$ (water), and it can also vary depending on the frequency of the electromagnetic fields (Keller, 1987).

For most of the Earth materials and for the air, the magnetic permeability μ can be approximated to its value in a vacuum, $\mu_0 = 4\pi \cdot 10^{-7}$ H/m. However, in highly magnetised materials this value can be greater, for example, due to an increase in the magnetic susceptibility just below the Curie point temperature (Hopkinson effect, e.g. Radhakrishnamurty and Likhite, 1970).

Across a discontinuity between two materials, named 1 and 2, the boundary conditions to be applied to the electromagnetic fields and currents described by Maxwell's equations are:

$$\hat{n} \times (\vec{E}_2 - \vec{E}_1) = 0\,, \tag{1.3a}$$

$$\hat{n} \times (\vec{H}_2 - \vec{H}_1) = \vec{j}_S\,, \tag{1.3b}$$

$$\hat{n} \cdot (\vec{D}_2 - \vec{D}_1) = \rho_S\,, \tag{1.3c}$$

$$\hat{n} \cdot (\vec{B}_2 - \vec{B}_1) = 0\,, \tag{1.3d}$$

$$\hat{n} \cdot (\vec{j}_2 - \vec{j}_1) = 0\,, \tag{1.3e}$$

where $\hat{n}$ is the unit vector normal to the discontinuity boundary, $\vec{j}_S$ (A/m^2) is the current density along the boundary surface and ρ_S (C/m^2) is the surface charge density. In the absence of surface currents, and considering constant values of ε and μ, only the tangential component of $\vec{E}$ and the normal component of $\vec{j}$ are continuous, whereas both the tangential and normal components of $\vec{B}$ are continuous across the discontinuity.

Due to the nature of the electromagnetic sources used in MT, the properties of the Earth materials and the depth of investigations considered, two hypotheses are applicable:

a) Quasi-stationary approximation: Displacement currents ($\partial \vec{D} / \partial t$) can be neglected relative to conductivity currents ($\vec{j}$) (eq. 1.1b) for the period range 10^{-5} s to 10^{5} s [1] and for not extremely low conductivity values. Therefore, the propagation of the electromagnetic fields through the Earth can be explained as a diffusive process, which makes it possible to obtain responses that are volumetric averages of the measured Earth conductivities.
b) Plane wave hypothesis: The primary electromagnetic field is a plane wave that propagates vertically towards the Earth surface (z direction) (Vozoff, 1972).

[1] In MT, the terms angular frequency (ω), frequency (f) and period (T) are employed. ω is mainly used in Maxwell's equations and in both the time and the frequency domains. f (s^{-1}=Hz) and T(s) are used mostly in the frequency domain, and the choice of using one or another depends usually on the studied frequency (or period) range. In this thesis, ω will be used mainly for theoretical developments and T for data treatment. The relationships between these three magnitudes are: $\omega = 2\pi f$ and $T = 1/f$.

The searched solutions of the electromagnetic fields from Maxwell's equations can be expressed through a linear combination of harmonic terms:

$$\vec{E} = \vec{E}_0 \cdot e^{i(\omega t + \vec{k}\vec{r})}, \tag{1.4a}$$

$$\vec{B} = \vec{B}_0 \cdot e^{i(\omega t + \vec{k}\vec{r})}, \tag{1.4b}$$

where ω (rad/s) is the angular frequency of the electromagnetic oscillations, t (s) is the time, $\vec{k}$ (m^{-1}) and $\vec{r}$ (m) are the wave and position vectors respectively. In both expressions, the first term in the exponent corresponds to wave oscillations and the second term represents wave propagation.

Using these harmonic expressions of the electromagnetic fields (eqs. 1.4a and 1.4b) and their constitutive relationships (eqs. 1.2a to 1.2c), if MT hypothesis a) (quasi-stationary approximation) is applied, Maxwell's equations in the frequency domain are obtained:

$$\vec{\nabla} \times \vec{E} = -i\omega\vec{B}, \tag{1.5a}$$

$$\vec{\nabla} \times \vec{B} = \mu_0 \sigma \vec{E}, \tag{1.5b}$$

$$\vec{\nabla} \cdot \vec{E} = \frac{\rho_V}{\varepsilon}, \tag{1.5c}$$

$$\vec{\nabla} \cdot \vec{B} = 0, \tag{1.5d}$$

where the value of the magnetic permeability (μ) is considered equal to the value in a vacuum (μ_0).

In the absence of charges, the right term of eq. 1.5c vanishes, and the electric and magnetic field solutions depend solely upon angular frequency (ω) and conductivity (σ).

Finally, using hypothesis b) (plane wave) and applying the boundary conditions (eqs. 1.3a to 1.3e) across discontinuities, the solutions of Maxwell's equations can be obtained.

In the case of an homogeneous structure, the components of the electric and magnetic fields take the form:

$$A_k = A_{k0} \cdot e^{i\omega t} \cdot e^{-i\alpha z} \cdot e^{-\alpha z}, \tag{1.6}$$

with $\alpha = \sqrt{\mu_0 \sigma \omega / 2}$ (m^{-1}). The first factor of the equation is the wave amplitude, the second and third factors (imaginary exponentials) are sinusoidal time and depth variations respectively and

the fourth is an exponential decay. This decay can be quantified by the skin depth, δ, the value of z for which this term decays to 1/e (Vozoff, 1991):

$$\delta = \sqrt{2/\mu_0 \sigma \omega} \approx 500\sqrt{\rho T} \quad (m) . \tag{1.7}$$

The skin depth permits the characterisation of the investigation depth, which, as can be seen, increases according to the square root of the product of medium resistivity and period. Although it has been defined for homogeneous media, its use can be extended to heterogeneous cases as well (e.g. geologic structures).

1.3 Magnetotelluric Transfer Functions

Magnetotelluric transfer functions (MTFs) or magnetotelluric responses are functions that relate the registered electromagnetic field components at given frequencies.

The MTFs depend only on the electrical properties of the materials and not on the electromagnetic sources. Hence, they characterise the conductivity distribution of the underlying materials according to the measured frequency.

The MTFs used in this thesis are the Impedance and Magnetotelluric Tensors and the Geomagnetic Transfer Function.

1.3.1 Impedance Tensor and Magnetotelluric Tensor

The *impedance tensor*, $\underline{Z}(\omega)$ (Ω), is a second-rank tensor (2x2 components). It relates the horizontal complex components of the electric ($\vec{E}$) and magnetic ($\vec{H} = \vec{B}/\mu_0$) fields at a given frequency (ω) (Cantwell, 1960):

$$\begin{pmatrix} E_x(\omega) \\ E_y(\omega) \end{pmatrix} = \begin{pmatrix} Z_{xx} & Z_{xy} \\ Z_{yx} & Z_{yy} \end{pmatrix} \cdot \begin{pmatrix} B_x(\omega)/\mu_0 \\ B_y(\omega)/\mu_0 \end{pmatrix} . \tag{1.8}$$

Weaver *et al.* (2000) introduced the term *magnetotelluric tensor*, $\underline{M}(\omega)$ (m/s), which uses $\vec{B}$ instead of $\vec{H}$ to define the relationships between the field components:

$$\begin{pmatrix} E_x(\omega) \\ E_y(\omega) \end{pmatrix} = \begin{pmatrix} M_{xx} & M_{xy} \\ M_{yx} & M_{yy} \end{pmatrix} \cdot \begin{pmatrix} B_x(\omega) \\ B_y(\omega) \end{pmatrix}. \tag{1.9}$$

In this thesis the use of the magnetotelluric tensor (MT tensor) is preferred, since it defines most of the parameters utilized [(2)].

The components of $\underline{M}$, M_{ij} (ij=xx,xy,yx,yy), are also complex magnitudes. Their expressions are M_{ij}=Re(M_{ij})+i·Im(M_{ij}) in Cartesian form and $M_{ij} = \left|M_{ij}\right| e^{i\varphi}$ in polar form.

From the modulus and phase of the polar expression of M_{ij}, two scalar magnitudes, which are real and frequency-dependent, are defined:

1) The apparent resistivity, which is an average resistivity for the volume of Earth sounded at a particular period:

$$\rho_{ij}(\omega) = \frac{\mu_0}{\omega}\left|M_{ij}(\omega)\right|^2 (\Omega \cdot m). \tag{1.10}$$

2) The impedance phase (or simply phase) is the phase of the M_{ij} component. It provides additional information on the conductivity of structures:

$$\varphi_{ij}(\omega) = \arctan\left(\frac{\mathrm{Im}\left(M_{ij}(\omega)\right)}{\mathrm{Re}\left(M_{ij}(\omega)\right)}\right). \tag{1.11}$$

1.3.2 Geomagnetic Transfer Function

The Geomagnetic Transfer Function (also known as the tipper vector or, tipper), $\vec{T}$, is a dimensionless complex vectorial magnitude, $\vec{T} = \mathrm{Re}(\vec{T}) + i \cdot \mathrm{Im}(\vec{T})$, and is defined as the relation between the vertical and the two horizontal components of the magnetic field:

$$B_z(\omega) = \left(T_x(\omega), T_y(\omega)\right) \cdot \begin{pmatrix} B_x(\omega) \\ B_y(\omega) \end{pmatrix}. \tag{1.12}$$

[2] $\underline{Z}$ and $\underline{M}$ are related to $\vec{H}$ and $\vec{B}$ through $\underline{Z} = \mu_0 \underline{M}$. In the literature and in the usual codes sometimes $\underline{M}$ is used instead of $\underline{Z}$, although it is referred to as $\underline{Z}$.

The tipper vector can be decomposed into two real vectors in the xy plane, corresponding to its real and imaginary parts. These real vectors are called induction vectors or induction arrows, and represent a projection of the vertical magnetic field on the horizontal xy plane. They are used to infer the presence of lateral variations in conductivity.

$$\vec{T}_{re}(\omega)=\left(\mathrm{Re}\left(T_x\right),\mathrm{Re}\left(T_y\right)\right), \tag{1.13}$$

$$\vec{T}_{im}(\omega)=\left(\mathrm{Im}\left(T_x\right),\mathrm{Im}\left(T_y\right)\right). \tag{1.14}$$

The graphical representation of the real induction arrows can be reversed (Parkinson convention) or non-reversed (Schmucker or Weise convention). Using the Parkinson convention the real induction arrow points to concentrations of currents, i.e., to more conductive zones.

1.4 Earth MT Dimensionality Models

The MT transfer functions, and particularly the relationships between their components, are reduced to specific expressions depending on the spatial distribution of the electrical conductivity being imaged. These spatial distributions, known as geoelectric dimensionality, can be classified as 1D, 2D or 3D. Other particular expressions of the transfer functions can be obtained when data are affected by galvanic distortion, a phenomenon caused by minor scale (local) inhomogeneities near the Earth's surface.

This section presents a summary of the characteristics of the different types of geoelectric dimensionality, regarding its geometry, the behaviour of the electromagnetic fields through them and the expressions of the related transfer functions. Galvanic distortion is also explained along with the type of transfer functions associated with this phenomenon.

1.4.1 1D

In this case the conductivity distribution is depth dependent only ($\sigma=\sigma(z)=1/\rho(z)$) and Maxwell's equations can be analytically solved by properly applying the boundary conditions (eqs. 1.3a to 1.3e). The solutions are electromagnetic waves, with the electromagnetic field always orthogonal to the magnetic field, that travel perpendicular to the surface of the Earth in a constant oscillation direction. They attenuate with depth depending on their period and conductivity values (eq. 1.7).

As a result, the MT transfer functions are independent of the orientation of the measured axes and are a function only of the frequency.

The magnetotelluric tensor is a non-diagonal tensor (diagonal elements = 0) with its two components equal in modulus but with opposite signs:

$$\underline{M}_{1D}(\omega) = \begin{pmatrix} 0 & M(\omega) \\ -M(\omega) & 0 \end{pmatrix}, \tag{1.15a}$$

with the corresponding resistivity and phases:

$$\rho_{xy}(\omega) = \rho_{yx}(\omega) = \frac{\mu_0}{\omega}\left|M(\omega)\right|^2 \left(\Omega \cdot m\right), \tag{1.15b}$$

$$\varphi(\omega) = \arctan\left(\frac{\mathrm{Im}\left(M\left(\omega\right)\right)}{\mathrm{Re}\left(M\left(\omega\right)\right)}\right), \tag{1.15c}$$

$$\varphi_{yx}(\omega) = \varphi_{xy} - \pi\,. \tag{1.15d}$$

The simplicity of the components of the magnetotelluric tensor allows working with only two scalar frequency-dependent quantities: These being the scalar apparent resistivity and phase:

$$\rho_{app}(\omega) = \rho_{xy}(\omega) = \rho_{yx}(\omega) \quad \left(\Omega \cdot m\right), \tag{1.15e}$$

$$\varphi_{app}(\omega) = \varphi_{xy}(\omega)\,. \tag{1.15f}$$

For the particular case of a half-space homogeneous Earth with conductivity σ (= 1/ρ), the MT tensor is frequency-independent and takes the form of eq. 1.15a, with $\mathrm{Re}(M) = \mathrm{Im}(M) = \sqrt{\rho\omega/2\mu_0}$. The apparent resistivity is equal to the resistivity of the medium, ρ. The impedance phase is 45^o.

With regard to the tipper, there is not a net component of the vertical magnetic field, B_z, due to the assumption that the incidence of the electromagnetic fields is perpendicular to the Earth's surface, and the fact that in a 1D model these fields do not change direction with depth. Therefore, the two components of the tipper, T_x and T_y are zero.

1.4.2 2D

In a two-dimensional Earth the conductivity is constant along one horizontal direction while changing both along the vertical and the other horizontal directions. The direction along which the conductivity is constant is known as the *geoelectrical strike* or *strike*. In the following

description, it is considered that the strike direction is parallel to the x axis (x ≡ x', i.e. $\theta = 0^o$) of the reference frame used in an MT survey (Figure 1.2) and therefore the variations of σ occur along y and z axes: σ(y,z).

In these cases, there is an induced vertical magnetic field, B_z, and Maxwell's equations can be decoupled into two modes, each one relating 3 different electric and magnetic perpendicular components:

Mode xy (E_x, B_y, B_z), also known as Transversal Electric (TE) mode, with currents (electric fields) parallel to the strike direction:

$$\frac{\partial E_x}{\partial z} = -i\omega B_y , \tag{1.16a}$$

$$\frac{\partial E_x}{\partial y} = i\omega B_z , \tag{1.16b}$$

$$\frac{\partial B_z}{\partial y} - \frac{\partial B_y}{\partial z} = \mu_0 \sigma E_x . \tag{1.16c}$$

Mode yx (B_x, E_y, E_z), or Transversal Magnetic (TM) mode, with currents perpendicular to the strike:

$$\frac{\partial E_y}{\partial z} - \frac{\partial E_z}{\partial y} = i\omega B_x , \tag{1.17a}$$

$$\frac{\partial B_x}{\partial z} = \mu_0 \sigma E_y , \tag{1.17b}$$

$$\frac{\partial B_x}{\partial y} = -\mu_0 \sigma E_z . \tag{1.17c}$$

The magnetotelluric tensor $\underline{M}$ in 2D models is non-diagonal and may be expressed as:

$$\underline{M}_{2D}(\omega) = \begin{pmatrix} 0 & M_{xy}(\omega) \\ M_{yx}(\omega) & 0 \end{pmatrix} = \begin{pmatrix} 0 & M_{TE}(\omega) \\ M_{TM}(\omega) & 0 \end{pmatrix}, \tag{1.18a}$$

where M_{xy} (E_x/B_y) and M_{yx} (E_y/B_x) come from TE and TM sets of equations respectively, and usually have opposite signs.

The values of the apparent resistivities and phases for xy and yx have different values and can be computed from eqs. 1.10 and 1.11. Since M_{xy} and M_{yx} have opposite signs, xy and yx phases belong to the 1st and 3rd quadrants.

The tipper is different from zero, and is related to the horizontal component y of the magnetic field, i.e., to the TE mode (eq. 1.16c):

$$\overline{T}_{2D}(\omega) = \left(0, T_y\right) = (0, B_z / B_y)\,. \tag{1.18b}$$

Both the real and imaginary induction arrows are oriented perpendicular to the strike direction (in this case x), and, according to Parkinson convention, point towards the zone of maximum conductivity.

In a 2D Earth, the measurements are, in general, not performed in the strike reference frame (x ≠ strike direction) because this is not known *a priori*. As a consequence, the magnetotelluric transfer functions cannot be expressed as in eqs. 1.18a and 1.18b.

However, it is possible to rotate the measuring axes an angle θ (strike angle) through the vertical axis, so the diagonal components of the magnetotelluric tensor become zero and the new x' axis is parallel to the geoelectrical strike. In the rotated reference frame (x', y', z) the rotated transfer functions are $\underline{M}'$ and T':

$$\underline{M}'(\omega) = R_\theta \cdot \underline{M}(\omega) \cdot R_\theta^T\,, \tag{1.19}$$

$$\overline{T}'(\omega) = R_\theta \cdot \overline{T}(\omega)\,, \tag{1.20}$$

where R_θ is a clockwise rotation matrix:

$$R_\theta = \begin{pmatrix} \cos\theta & \sin\theta \\ -\sin\theta & \cos\theta \end{pmatrix}, \tag{1.21}$$

and R_θ^T its transpose.

In the rotated reference frame (x', y', z), TE and TM modes can be equally defined according to the strike direction.

The retrieval of the strike angle from the MT tensor can be done using several methods that will be reviewed in the next chapter. It is important to note that this retrieval has 90^o of ambiguity, which can be solved through the information given by the tipper vector, the variation of MT responses along different locations and geology.

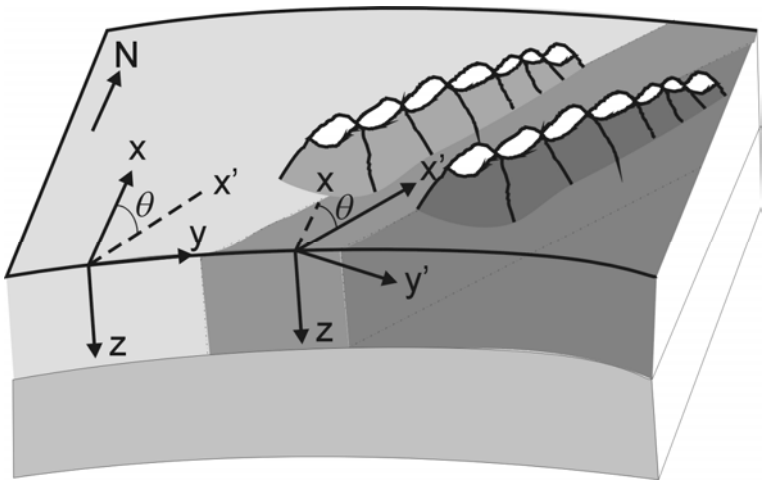

Figure 1.2: Sketch of an Earth model with reference frame axes used in an MT survey and in the analyses of their responses. (x, y, z): measurement system coordinates. x and y are the horizontal axes, where x usually points towards North and y points towards East. The z axis points vertically inward. Commonly, a reference frame rotated around the z axis (x', y', z) is also used. θ indicates the angle between the x' and x axes.

1.4.3 3D

This is the most general type of geoelectrical structure. Here, the conductivity changes along all directions ($\sigma = \sigma(x,y,z)$). In this case, Maxwell's equations can not be separated into two modes.

MT transfer functions take the general forms with all components non-zero (eqs. 1.9 to 1.14), because M_{xx} and M_{yy} are not null. There is not any rotation direction through which the diagonal components of the magnetotelluric tensor or any component of the tipper vector can vanish.

1.4.4 The Galvanic Distortion Phenomenon

Distortion in magnetotellurics is a phenomenon produced by the presence of shallow and local bodies or heterogeneities, which are much smaller than the targets of interest and skin depths. These bodies cause charge distributions and induced currents that alter the magnetotelluric responses at the studied or regional scale (Kaufman, 1988; Chave and Smith, 1994). In the case that these bodies are of the same proportions as the interest depth, they can be modeled in a 3D environment.

Distortion can be inductive or galvanic. Inductive distortion is generated by current distributions, has a small magnitude and decays with the period. Under the condition $\sigma >> \omega\varepsilon$ (quasi-stationary approximation) it can be ignored (Berdichevsky and Dmitriev, 1976).

Galvanic distortion is caused by charge distributions accumulated on the surface of shallow bodies, which produce an anomalous electromagnetic field. This anomalous magnetic field is small, whereas the anomalous electric field is of the same order of magnitude as its regional counterpart and is frequency-independent (Bahr, 1988; Jiracek, 1990). Hence the galvanic distortion is treated as the existence of an anomalous electric field, $\vec{E}_a$.

Mathematically, the effect of this electric field on the transfer functions can be represented by a 2x2 real, frequency-independent and non-dimensional matrix, *C* (Berdichevsky and Dmitriev, 1976):

$$C = \begin{pmatrix} C_1 & C_2 \\ C_3 & C_4 \end{pmatrix}. \tag{1.22}$$

The elements of *C* depend on the geometry and position of the distorting body as well as on the resistivity contrast between the body and the surrounding medium (Jiracek, 1990).

The magnetotelluric tensor that accounts for the measurement of the regional and distorted fields is then:

$$\underline{M}_m(\omega) = C \cdot \underline{M}_R(\omega), \tag{1.23}$$

where $\underline{M}_m$ is the measured tensor and $\underline{M}_R$ is the regional tensor, which corresponds to the regional structure. Also, $\underline{M}_m$ can have been measured in a reference frame rotated an angle α with respect to the regional reference frame:

$$\underline{M}_m(\omega) = R_\alpha \cdot C \cdot \underline{M}_R(\omega) \cdot R_\alpha^T. \tag{1.24}$$

The effects of galvanic distortion depend on the type of dimensionality of the regional media.

In the case of a 1D regional Earth, galvanic distortion produces a constant displacement of the apparent resistivity along all frequencies. This is known as *static shift*, and does not affect the phases. A static shift also occurs in a 2D Earth with one of the measurements axes aligned with the strike direction. Although it seems to be a minor problem, static shift represents one of the main handicaps in the analysis of MT responses. There is no a general analytical or numerical way to model the cause of static shift and thus to correct it by using MT itself. This makes it necessary to use information from other methods that are less affected (TEM) or to compare the responses with geological information. Some proposals to correct static shift can be

found in Jones (1988) and Ogawa (2002), and new methods are being developed (Ledo *et al.*, 2002a; Tournerie *et al.*, 2004; Meju, 2005).

In contrast, if distortion affects a 2D tensor rotated a certain angle θ from the strike direction, or a 3D structure, both phases and resistivities are affected with a dependence on the frequency.

Since the main target of interest in a MT survey is the regional structure and not the distorting bodies, different decomposition techniques exist to remove the effects of distortion and recover the regional responses.

There are different methods to correct galvanic distortion over one-dimensional and two-dimensional structures (Zhang *et al.*, 1987; Bahr, 1988; Groom and Bailey, 1989 and Smith, 1995). These methods consider a galvanic distortion affecting a 2D regional structure, with the magnetotelluric tensor measured in a reference frame that is rotated an angle θ from the regional strike:

$$\underline{M}_m = R_\theta \cdot C \cdot \underline{M}_{2D}(\omega) \cdot R_\theta^T . \tag{1.25}$$

In the method proposed by Groom and Bailey (1989) the distortion is described by the contribution of four effects, represented by the gain (g) parameter, which accounts for the static shift, and the twist (φ_t), shear (φ_e) and anisotropy (φ_s) angles or their tangents (t, e and s respectively):

$$C = g \cdot \begin{pmatrix} (1+s)(1-te) & (1-s)(e-t) \\ (1+s)(e+t) & (1-s)(1+te) \end{pmatrix}. \tag{1.26}$$

Alternatively, Smith (1995) uses two gain parameters, g_1 and g_2, and two distortion angles, ϕ_1 and ϕ_2:

$$C = \begin{pmatrix} g_1 \cos\phi_1 & -g_2 \sin\phi_2 \\ g_1 \sin\phi_1 & g_2 \cos\phi_2 \end{pmatrix}. \tag{1.27}$$

The relationships between both sets of parameters are:

$$g_{\substack{1 \\ 2}} = g(1 \pm s), \tag{1.28}$$

$$\phi_{\substack{1 \\ 2}} = \varphi_t \pm \varphi_e . \tag{1.29}$$

An alternative decomposition of the galvanic distortion matrix is shown in Appendix F.

The aim of these decomposition methods is to solve a linear system of equations (8 equations) that allow determining the values of the distortion parameters, the strike angle and the regional magnetotelluric tensor components (9 parameters in total). The gain (static shift) remains unknown and additional information is necessary to retrieve its value. McNeice and Jones (2001) developed the Multisite Multifrequency tensor decomposition code (Strike), which, based on a statistical approach, retrieves twist and shear distortion parameters in accordance with a 2D regional model with a unique strike direction.

In three-dimensional geoelectric structures it is not easy to perform the decomposition unless the characteristics of the distortion are well known. In these cases, several approaches have been proposed to correct galvanic distortion over regional 3D structures (Ledo *et al.*, 1998; Garcia and Jones, 1999; Utada and Munekane, 2000).

In the most general cases, it is not possible to discern whether data are affected or not by galvanic distortion and the type of regional structure. Further analyses must be carried out to obtain such information, commonly based on the use of the invariant parameters of the magnetotelluric tensor.

1.5 Electromagnetic Sources in MT

"The dependence of MT on natural fields is both its major attraction and its greatest weakness" (Vozoff, 1991).

The electromagnetic oscillations of interest in magnetotellurics have a period range from about 10^{-5} s to 10^{5} s, which belong to the lowest part of the known electromagnetic spectrum, from the long radio waves ($\lambda \approx 1$ km) to $\lambda \approx 10^{10}$ km (Figure 1.3). These frequencies permit range of investigation depths from ten meters to hundreds of kilometres. The natural phenomena that generate the electromagnetic fields with these frequencies are thunderstorm activity world-wide and the interaction between the solar wind and the Earth's magnetosphere.

For periods shorter than 1s, lightning discharges are the main source of electromagnetic waves. The energy released from lightning at a frequency of about 8 Hz (Schuman resonance) and its multiple harmonics up to 2000 Hz are trapped in an insulating waveguide between the conductive Earth and the conductive ionosphere, such that this energy can travel for long distances. It is estimated that occurrences of lightning somewhere in the world (from 100 to 1000 per second) is sufficient to have a continuous energy source at any location over the Earth's surface (Malan, 1963; Kaufman and Keller, 1981; Vozoff, 1991). In MT, measurements in the range from 10^{5} Hz to 1 Hz are referred to as Audiomagnetotellurics (AMT).

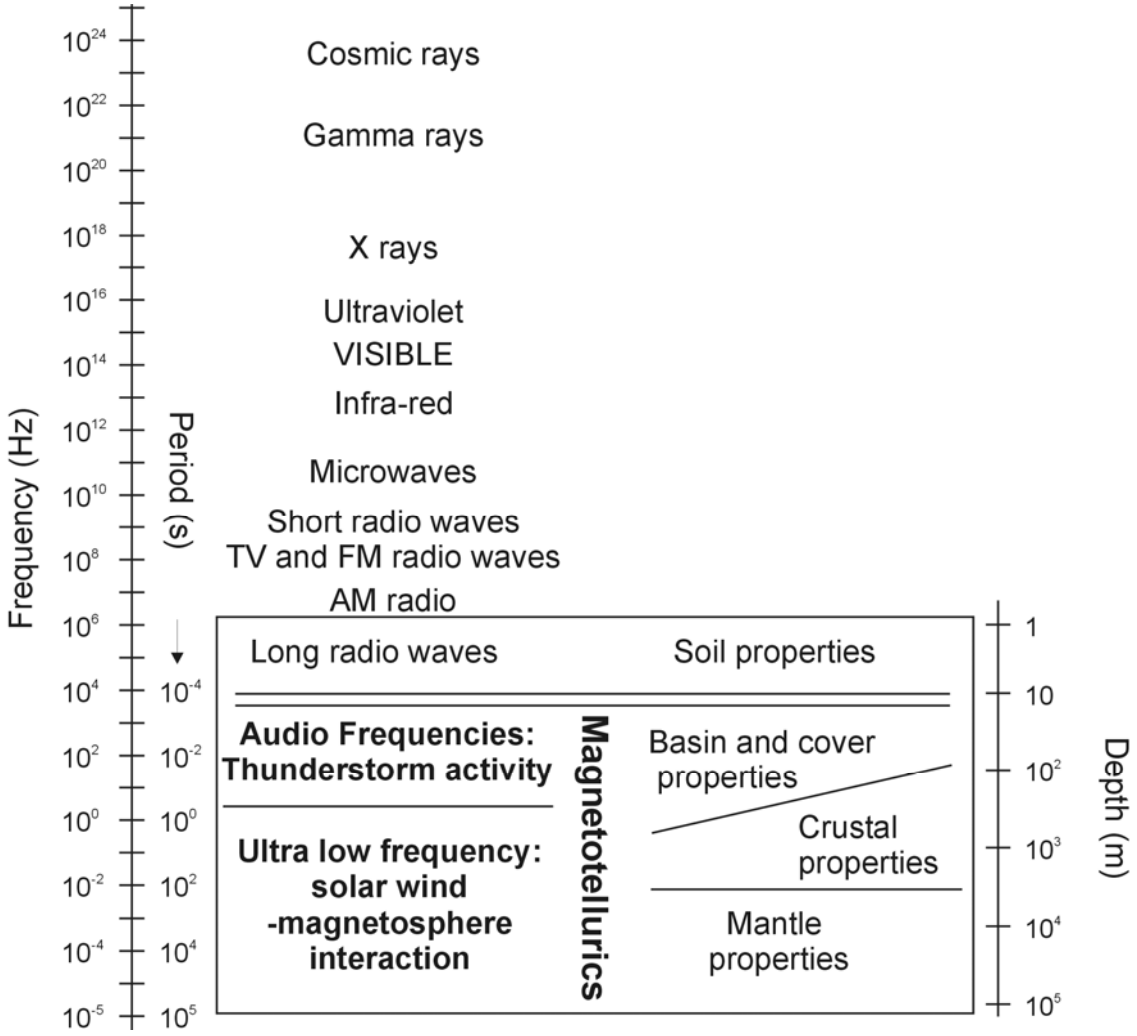

Figure 1.3: Schematic representation of the known electromagnetic spectrum. The box corresponds to the part of the spectrum used in magnetotellurics, where the MT sources, targets and investigation depths are indicated.

For periods from 1 s to 10^5 s, the electromagnetic activity is dominated by hydro-magnetic waves in the Earth's magnetosphere, mainly generated by the solar wind (Campbell, 2003; McPherron, 2005). The solar wind consists of highly energetic ions ejected from the Sun and its magnetic field, which interact with the Earth's magnetic field, changing its intensity and geometry. Within the Earth's magnetosphere, the ionosphere is an atmospheric layer between 100 km and 1000 km of altitude. It is highly conductive because its particles are ionised by ultraviolet and other solar radiation. The interaction between the solar wind and gases in the ionosphere result in several processes (McPherron, 2002) that produce an electromagnetic field. The field travels through the lower layers of the atmosphere and reaches the Earth surface. This interaction is also responsible for the Northern and Southern lights, visible at high latitudes. At these latitudes, auroral effects must be corrected to satisfy the MT method hypotheses (Pirjola,

1992; Garcia *et al.*, 1997). When MT measurements are made at low latitudes, the effects of the equatorial electrojet, an Eastward current caused by the Earth's magnetic field being horizontal at these latitudes (Padilha, 1999; Campbell, 2003), can be important and must be corrected also.

Around 1 s, in the limit between thunderstorm activity and solar wind – ionosphere interaction, there is a narrow period range (0.2 s - 2 s), known as the dead band, in which the power spectrum of the natural electromagnetic field has a minimum (Figure 1.4) that produces low-amplitude MT signals.

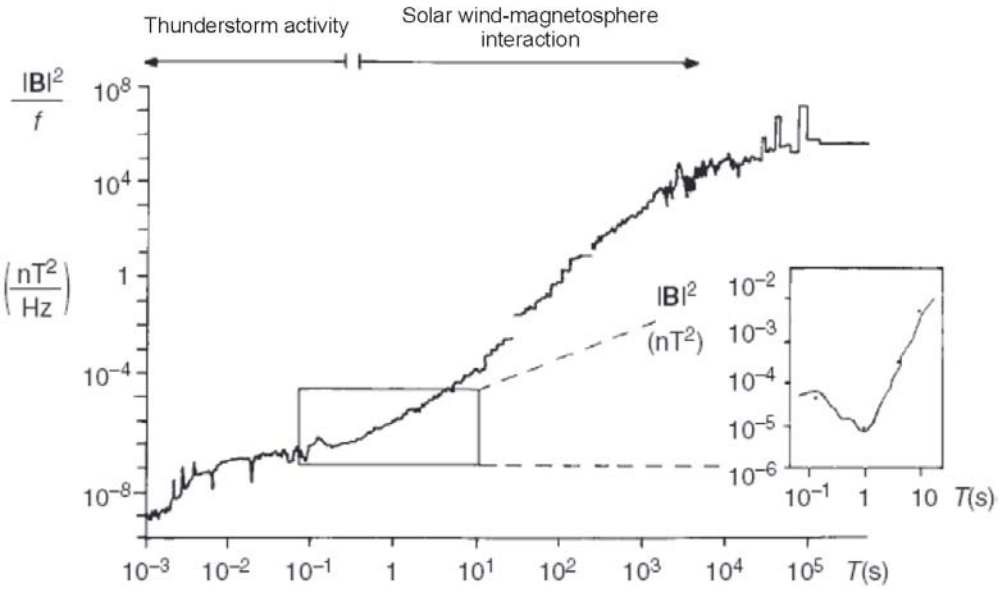

Figure 1.4: Power spectrum of natural magnetic field variations. The inset depicts the minimized signal power in the dead band. (Modified from Junge, 1996).

To these two natural sources, other electromagnetic signals can be added, known as noise. In terms of data processing, noise can be defined as that part of the data which cannot be explained by the framework of a theory (Junge, 1996). In general, any factor, which makes the MT method assumptions invalid, is considered noise. The sources of electromagnetic noise can be instrumental, environmental (seismic, electromagnetic signals of no interest in Earth studies, biological) as well as cultural or man-made noise (electric devices, power stations and lines, railways, electric fences, radio and TV transmitters...). The effects of noise could be minimised by the use of filters in the acquisition instruments, accurate signal processing methods (see section 1.7) and the use of one or more remote references (Gamble *et al.*, 1979).

Below 10^{-4} s, the natural electromagnetic signal is very weak and other types of electromagnetic sources are needed in order to effectively explore the shallow subsurface. This

is achieved by Controlled Source Audio Magnetotellurics (CSAMT), consisting of the use of antennas radiating at short periods, such that MT theory assumptions are fulfilled (Zonge and Hughes, 1991).

1.6 Instrumentation

The equipment necessary for MT data acquisition consists of sensors that measure the electric and magnetic field components (channels) and one data logger that controls and performs the acquisition process and the data storage.

The electric field components E_x and E_y are indirectly measured through the potential difference ΔV between two electrodes separated a distance d along the desired direction: $\Delta V = E_i / d$. Both electrodes stay in contact with the soil and are connected to the data logger that closes the circuit and stores the measured signal. The separation between the electrodes must guarantee enough voltage to be registered by the data logger, and also account for the fact that the voltage decreases as a function of period. The sensitivity of the acquisition systems used at present allows a separation of 10 m – 20 m for AMT frequencies and 50 m – 100 m for the rest. In any case, the choice of the distance is many times limited by the topography of the terrain. Within the AMT frequency range steel electrodes are used. Outside this range the electrodes must be non-polarisable to avoid additional electrochemical currents. Normally, these electrodes consist of a KCl or $PbCl_2$ solution in a ceramic container that is designed to ensure a good contact between the outside wires and the soil.

For the magnetic field, the most commonly used sensors are induction coils. According to the Faraday-Lenz law, under a magnetic flux time variation, an electromotive force (*emf* (V)) is induced in a coil. Coils must be oriented along the direction of the component to be measured (usually B_x, B_y and B_z). The number of loops in the magnetometers must be in agreement with the induced *emf*, which decreases along with the period. Nowadays, the same size coil is valid for a broad range of periods, and the data must be posteriorly calibrated according to their sensitivity to the different voltage values. At very long periods, another type of magnetic sensor, the flux magnetometer, is used.

The data logger (e.g. Figure 1.5) is the control unit of the MT measuring system. It controls the acquisition process, filters and amplifies the sensors signals and converts these data into digital format through an A/D converter.

The sensors' signals are stored in the data logger using a certain sampling frequency, which, according to Nyquist theorem, must be at least twice the value of the highest frequency to be evaluated. In order to avoid an oversampling of the longest period data to save disk space

and aliasing, the data acquisition process is separated into several frequency bands, each one with a different sampling frequency. This acquisition in data bands also permits adaptation of the A/D converter to the signal amplitudes and to the sensors' sensitivities at the given band.

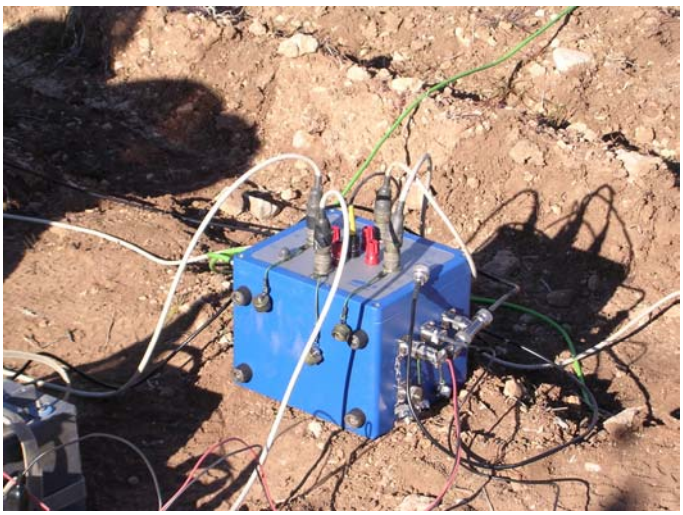

Figure 1.5: Metronix ADU-06 data logger.

Table 1.1: presents the recording bands of the Metronix ADU-06 system, one of the systems used in this study. In this system, the data at a given band can be obtained by the use of low-pass filters during recording (bands HF, LF1, LF2 and Free) or by a posterior sampling of the final time series (bands LF3, LF4 and LF5).

Band	Sampling frequency/period	Frequency/period range
HF	40960 Hz	20000 Hz – 500 Hz
LF1	4096 Hz	1000 Hz - DC
Free	128, 256, 512, 1024 or 2048 Hz	60, 120, 240, 480 or 960 Hz to DC
LF2	64 Hz	30 Hz – DC
LF3	2 Hz	0.9 Hz – DC
LF4	2 s or 16 s	5s or 35s to DC
LF5	8 s, 64 s or 512 s	20s, 150s or 1200s to DC

Table 1.1: Recording bands for the Metronix ADU-06 system, indicating their corresponding sampling frequency/period and recorded ranges.

1.7 Time Series Processing

1.7.1. General overview

The MT transfer functions are obtained from time series processing of the acquired data. Commonly, processing is carried out separately for each measured band, involving three main steps: 1) data set up and preconditioning, 2) time to frequency domain conversion and 3) estimation of the magnetotelluric transfer functions.

1) Data set up and preconditioning

The recorded time series are divided into M segments containing N samples each. The value of N is chosen depending on the recorded band such that each segment contains an elevated number of periods. In addition, each band must be divided into a sufficient number of segments for further statistical estimation of the transfer functions.

Once the segments have been defined, they are inspected in order to identify and remove trends and noise effects (spikes). This is performed manually and/or automatically using specific software.

2) Time to frequency domain conversion

From each segment, the measured channels E_i (i=x,y) and B_j (j=x,y,z) are converted from time to frequency domain using the Discrete Fourier Transform (Brigham, 1974) or Cascade Decimation (Wight and Bostick, 1980), both based on the Fast Fourier Transform (FFT), or using the Wavelet transform (Zhang and Paulson, 1997; Trad and Travassos, 2000; Arango, 2005). Hence, a raw spectrum with N/2 frequencies is obtained. From these, evaluation frequencies, equally distributed in a logarithmic scale, optimally 6-10 per period decade, are chosen. The final spectra are smoothed by averaging over neighbouring frequencies using a Parzen window function. Each field component must be calibrated according to the instrument sensitivity at a given frequency. The auto and cross spectra of a segment k, which are the products of the field components and their complex conjugates, are then obtained for each frequency: $E_{ki}(\omega)\cdot E^*_{ki}(\omega)$, $B_{kj}(\omega)\cdot B^*_{kj}(\omega)$, $E_{ki}(\omega)\cdot B^*_{kj}(\omega)$ and $B_{kj}(\omega)\cdot E^*_{ki}(\omega)$. These are stored in the so-called spectral matrix, which contains the contributions from all the segments at a specific frequency.

3) Estimation of the magnetotelluric transfer functions

The evaluation of the MT transfer functions from eqs. 1.9 and 1.12 needs at least two independent observations of the corresponding field components in the frequency domain, which can be obtained from two segments:

$$E_x(\omega) = M_{xx}(\omega)\cdot B_x(\omega) + M_{xy}(\omega)\cdot B_y(\omega)\,, \tag{1.30}$$

$$E_y(\omega) = M_{yx}(\omega)\cdot B_x(\omega) + M_{yy}(\omega)\cdot B_y(\omega)\,, \tag{1.31}$$

$$B_z(\omega) = T_x(\omega)\cdot B_x(\omega) + T_y(\omega)\cdot B_y(\omega)\,. \tag{1.32}$$

However, to solve these equations accurately, a larger number of segments is required, due to the presence of noise in the measured data as well as the fact that two segments may not contain all the evaluation frequencies. Hence, the transfer functions are evaluated after multiplying eqs. 1.30 to 1.32 by the conjugates of the horizontal magnetic field ($B_x^*(\omega)$ and $B_y^*(\omega)$). This allows obtaining six independent equations whose parameters are elements of the spectral matrix. The conjugates $B_x^*(\omega)$ and $B_y^*(\omega)$ are used, instead of other possible combinations of field components, as they have the highest degree of independence (Vozoff, 1972) and provide the most stable results:

$$M_{xx} = \frac{\left\langle E_x B_x^* \right\rangle \left\langle B_y B_y^* \right\rangle - \left\langle E_x B_y^* \right\rangle \left\langle B_y B_x^* \right\rangle}{DET_1}\,, \tag{1.33}$$

$$M_{xy} = \frac{\left\langle E_x B_x^* \right\rangle \left\langle B_x B_y^* \right\rangle - \left\langle E_x B_y^* \right\rangle \left\langle B_x B_x^* \right\rangle}{DET_2}\,, \tag{1.34}$$

$$M_{yx} = \frac{\left\langle E_y B_x^* \right\rangle \left\langle B_y B_y^* \right\rangle - \left\langle E_y B_y^* \right\rangle \left\langle B_y B_x^* \right\rangle}{DET_1}\,, \tag{1.35}$$

$$M_{yy} = \frac{\left\langle E_y B_x^* \right\rangle \left\langle B_x B_y^* \right\rangle - \left\langle E_y B_y^* \right\rangle \left\langle B_x B_x^* \right\rangle}{DET_2}\,, \tag{1.36}$$

$$T_x = \frac{\left\langle B_z B_x^* \right\rangle \left\langle B_y B_y^* \right\rangle - \left\langle B_z B_y^* \right\rangle \left\langle B_y B_x^* \right\rangle}{DET_1}\,, \tag{1.37}$$

$$T_y = \frac{\left\langle B_x B_x^* \right\rangle \left\langle B_z B_y^* \right\rangle - \left\langle B_x B_y^* \right\rangle \left\langle B_z B_x^* \right\rangle}{DET_1}\,, \tag{1.38}$$

where $DET_1 = \left\langle B_x B_x^* \right\rangle \left\langle B_y B_y^* \right\rangle - \left\langle B_x B_y^* \right\rangle \left\langle B_y B_x^* \right\rangle$ and $DET_2 = \left\langle B_y B_x^* \right\rangle \left\langle B_x B_y^* \right\rangle - \left\langle B_y B_y^* \right\rangle \left\langle B_x B_x^* \right\rangle$.

Cross and power spectra $<AB^*>$ are constructed from the individual segments k, through a variety of methods, all of which perform a segment selection to obtain an optimal estimation of the transfer functions.

The following is a summary of the most common methods for estimating TFs:

The first methods utilised least squares (LS) (Sims *et al.*, 1971), which minimises the quadratic sum of the difference between the measured fields and those computed from the MT transfer functions, assuming equally distributed Gaussian errors. These methods failed since the errors highly depend on the strength of the signal and are extremely sensitive to the presence of noise.

The magnetic remote reference acquisition method was introduced by Gamble *et al.* (1979) as a way to eliminate uncorrelated noise in the recorded fields. It is based on the fact that the magnetic field is stable over large distances and that the local noise recorded in the magnetic and electric fields can be detected and removed. It consists of the simultaneous recording of local and remote magnetic fields. The transfer functions are estimated as in eqs. 1.33 to 1.38, using the remote magnetic fields as the conjugate components.

Robust processing (Huber, 1981) consists of identifying and removing outliers to make estimates more "robust", which means that the estimates are not greatly affected by these outliers and respond slowly to the addition of more data. In the processing of magnetotelluric data, different robust methods have been developed:

- Egbert and Booker (1986) developed a robust method, similar to LS, with a weighting based on the errors, and the introduction of a "loss function" (Huber, 1981), which reduced the effect of outliers.
- Jones and Jödicke (1984) presented a coherence rejection technique, based on the maximisation of the field coherences (relationships between the estimated and predicted field components), using the jacknife approach (see chapter 3). A similar method is the variance minimisation technique (Jones *et al.*, 1989).
- Chave and Thomson (2004) developed a code to estimate the MT transfer functions (BIRRP: Bounded Influence Remote Reference Processing) which introduced the use of a bounded influence estimator to compare the measured and computed fields, and a hat matrix function to reduce the effects of outliers.

These three types of methods have been recently adapted to the use of single and multiple remote references.

The errors of the transfer functions are commonly estimated assuming that noise contributions are random and that the cross and power spectra from the individual segments follow a Gaussian distribution.

The variances of the MT tensor components are evaluated as (Bendat and Piersol,1971):

$$\mathrm{var}\left(M_{ij}\right)=\frac{4}{\nu-4}F_{0.68}\left(1-\gamma^2\right)\frac{\left\langle E_iE_i^*\right\rangle\left\langle B_jB_j^*\right\rangle}{DET_j}, \tag{1.39}$$

where ν is the number of degrees of freedom, $F_{0.68}(1-\gamma^2)$ is the upper limit of the Fisher-Schnedecor distribution for a given probability (68%), and γ^2 denotes the squared bivariate coherency between the predicted (P) and registered (R) field components:

$$\gamma^2(R,P)=\frac{\left\langle RP^*\right\rangle\left\langle PR^*\right\rangle}{\left\langle RR^*\right\rangle\left\langle PP^*\right\rangle}. \tag{1.40}$$

The error bars of the real and imaginary parts of the MT tensor components are equally determined to be the square root of the variance, which can be represented as a circle in the complex plane (Bendat and Piersol, 1971):

$$\delta(\mathrm{Re}\,M_{ij})=\delta(\mathrm{Im}\,M_{ij})=\delta(M_{ij})=(\mathrm{var}(M_{ij}))^{1/2}. \tag{1.41}$$

Through an error propagation process, the errors of the apparent resistivities and phases can also be estimated:

$$\delta(\rho_{ij})=2\frac{\delta(M_{ij})}{\left|M_{ij}\right|}\rho_{ij}=0.4T\left|M_{ij}\right|\delta(M_{ij}), \tag{1.42}$$

$$\delta\left(\varphi_{ij}\right)=\arcsin\frac{\delta\left(M_{ij}\right)}{\left|M_{ij}\right|}. \tag{1.43}$$

A similar development leads to the error estimation of the tipper components.

Commonly, the error bars of the apparent resistivities are obtained as log (ρ_{ij}) rather than ρ_{ij}, which produce symmetrical error bars in a logarithmic plot. The errors of the phases are also are approximated, to remove the arcsine dependence:

$$\delta\left(\log\rho_{ij}\right)=2\frac{d\log\left|M_{ij}\right|}{d\left|M_{ij}\right|}\delta\left(M_{ij}\right)=\frac{0.87}{\left|M_{ij}\right|}\delta\left(M_{ij}\right), \tag{1.44}$$

$$\delta(\varphi_{ij}) = \frac{0.71}{|M_{ij}|}\delta(M_{ij}) \quad .^{(3)} \tag{1.45}$$

1.7.2. Common processing techniques

At present, different processing software schemes are available, which implement some of the techniques explained above. In these, step 1) (data set up and preconditioning) is generally done automatically, using some of the windowing functions. The use of Cascade Decimation to transform the data from time to frequency domain (step 2) is almost generalised nowadays, as it presents important advantages over conventional FFT: less memory requirements, ability to compensate for rejected data in the time series, optimal results for broad band series and the conversion to frequencies in logarithmic scale.

With regard to the estimation of the MT transfer functions, robust methods with single (Jones *et al.*, 1989) and multiple (SAMTEX, 2004) remote references have been proven to give the best estimates.

However, when the data are highly affected by noise, these techniques may lead to similar, yet non-very satisfactory results, especially in the tipper function. It must be taken into account that each set of data has its particular characteristics and it is necessary to carefully inspect the time series, remove noisy segments in different ways and change some parameters in the windowing functions and the transfer functions estimation. Tools for quality control can be the coherency and the smoothness of the estimated functions.

---

[3] Proof:

Departing from the error of $\tan\varphi_{ij}$ ($\tan\varphi_{ij} = Im(M_{ij})/Re(M_{ij}) = y/x$):

$$\delta\left(\tan\varphi_{ij}\right) = \sqrt{\left(\frac{\partial\tan\varphi_{ij}}{\partial x}\right)^2\delta^2(x) + \left(\frac{\partial\tan\varphi_{ij}}{\partial y}\right)^2\delta^2(y)} = \sqrt{\left(\frac{-y}{x^2}\right)^2\delta^2(x) + \left(\frac{1}{x}\right)^2\delta^2(y)},$$

where, using eq. 1.41 ($\delta(x) = \delta(y) = \delta\left(M_{ij}\right)$): $\delta\left(\tan\varphi_{ij}\right) = \frac{y}{x}\sqrt{\left(\frac{1}{x^2} + \frac{1}{y^2}\right)\delta^2\left(M_{ij}\right)} \approx \tan\varphi_{ij}\cdot\sqrt{2}\frac{\delta\left(M_{ij}\right)}{|M_{ij}|}$.

On the other hand: $\delta\left(\tan\varphi_{ij}\right) = \left|\frac{d\tan\varphi_{ij}}{d\varphi_{ij}}\right|\delta\left(\varphi_{ij}\right) = \left|\frac{1}{\cos^2\varphi_{ij}}\right|\delta\left(\varphi_{ij}\right)$.

Equaling both errors: $\frac{1}{\cos^2\varphi_{ij}}\delta\left(\varphi_{ij}\right) = \tan\varphi_{ij}\cdot\sqrt{2}\frac{\delta\left(M_{ij}\right)}{|M_{ij}|}$,

and $\delta\left(\varphi_{ij}\right) = \tan\varphi_{ij}\cdot\cos^2\varphi_{ij}\cdot\sqrt{2}\frac{\delta\left(M_{ij}\right)}{|M_{ij}|} = \sin\varphi_{ij}\cdot\cos\varphi_{ij}\cdot\sqrt{2}\frac{\delta\left(M_{ij}\right)}{|M_{ij}|} = \frac{\sin 2\varphi_{ij}}{2}\sqrt{2}\frac{\delta\left(M_{ij}\right)}{|M_{ij}|}$.

Assuming an average angle $\varphi_{ij} = 45^{o}$, $\delta\left(\varphi_{ij}\right) = \frac{\sqrt{2}}{2}\frac{\delta\left(M_{ij}\right)}{|M_{ij}|}$. QED.

1.8 Modelling and Inversion of MT Data

The conductivity distribution of the Earth in the region of interest is usually obtained through a modelisation process. In MT, a model consists of a region with a particular conductivity distribution, which can be 1D, 2D or 3D depending on the conductivity variations along different directions. The model parameters are the conductivity values at different model positions. The model responses are normally the resistivities and phases measured at the Earth's surface as a consequence of the electromagnetic fields travelling through these conductivity distributions, according to Maxwell's equations, although other functions can be used.

Depending on the dimensionality and complexity associated with the magnetotelluric transfer functions, 1D, 2D and 3D models are constructed using different modelling techniques.

Nowadays, the forward modelling can be solved efficiently for any dimensionality model, analytically in simple cases and numerically in general. One of the most used codes in 2D is PW2D (Wannamaker *et al.*, 1987), which uses the finite elements algorithm to compute the model responses, and is characterised by high numerical stability. In 3D, the Mackie *et al.* (1993) code solves the integral form of Maxwell's equations using the finite differences method. The Pek and Verner (1997) code uses finite differences to solve the forward modelling problem for anisotropic structures.

Inversion schemes search the relationships between the measured data and the model responses, modifying the model until an agreement is approached. In many cases these are a combination of forward modelling plus minimisation (or maximisation) algorithms. OCCAM 1D and 2D inversion codes (Constable *et al.*, 1987) are based on the minimisation or maximisation of a certain function using a Lagrange multiplier. In 2D, the RRI (Rapid Relaxation Inversion) (Smith and Booker, 1991), RLM2DI (Mackie *et al.*, 1997) and REBOCC (Siripunvaraporn and Egbert, 2000) codes are in common usage. Pedersen and Engels (2005) developed the application of the REBOCC code (DetREBOCC) to invert the determinant of the impedance tensor.

In relation to 3D conductivity models, MT inversion is still in the development stage, although several algorithms tested with synthetic data and simple models have already led to satisfactory results. 3D inversion codes will be available in the near future (Mackie and Madden, 1993; Newman and Alumbaugh, 2000; Zhdanov *et al.*, 2000; Sasaki, 2001). One of these codes is Siripunvaraporn *et al.* (2005), based on the data-space method, as an extension of the Occam approach, which has recently been officially released to public. Meanwhile, 3D MT interpretation is done by trial-and-error forward model fitting.

Chapter 2: Geoelectric Dimensionality and Rotational Invariants of the Magnetotelluric Tensor

In the previous chapter the concept of geoelectric dimensionality was introduced. This chapter investigates further into its characterisation. It introduces the rotational invariants of the magnetotelluric tensor and presents the most common methods used to obtain a description of the dimensionality and the recovery of the regional tensor. Moreover, at the end of the chapter, the main problems and limitations existing in the dimensionality characterisation are discussed. Finally, the different aspects of the work performed in this thesis, which allow totally or partially solving some of these problems and limitations, are indicated.

2.1. Introduction

As explained in chapter 1, analysis of dimensionality is a powerful tool that may provide information such as variation of strike direction with depth, which can be correlated with different processes and structure in the Earth's crust and mantle (e.g. Marquis *et al.,* 1995). Depending on the result of dimensionality analysis, MT data may be interpreted as being either one, two or three-dimensional. A proper dimensionality interpretation is important since a two-dimensional interpretation of three-dimensional data can be acceptable in some cases while not in others (Wannamaker, 1999; Park and Mackie, 2000; Ledo *et al*., 2002b; Ledo, 2005).

Most of the methods used to decipher the dimensionality of the geoelectric structures are based on the rotational invariants, i.e., sets of parameters computed from the observed MT

tensor that do not depend on the direction of the measuring axes. Different sets of rotational invariants have been proposed to assert particular categories of dimensionality (Swift, 1967; Berdichevsky and Dmitriev, 1976; Bahr, 1988; Bahr, 1991; Lilley, 1993, 1998a, 1998b). Fischer and Masero (1994) argued the existence of eight invariants, seven independent and one dependent and, later, Szarka and Menvielle (1997) determined a full set of MT tensor invariants and suggested their use for a compact dimensionality interpretation. Weaver *et al.* (2000) provided a method whereby dimensionality was characterised in terms of the annulment of some of the invariants. Other authors (Romo *et al.*, 1999) use invariant parameters defined from the geomagnetic transfer function to characterise 2D and 3D responses.

Alternatively, Caldwell *et al.* (2004) introduced the magnetotelluric phase tensor, defined as the relationship between the real and imaginary parts of the MT tensor. It is a practical tool to obtain information about the dimensionality of the regional structure, since it is not affected by galvanic distortion. However, because of this, its applications are limited, since it is not possible to recover the regional responses.

2.2. Fundamental Rotational Invariants of the Magnetotelluric Tensor

Under a rotation of an arbitrary angle α around the z-axis, a reference frame xyz is transformed into x'y'z. Accordingly, the magnetotelluric tensor can be defined in the new reference frame: $\underline{M}'(\omega) = R_\alpha \cdot \underline{M}(\omega) \cdot R_\alpha^T$ (eq. 1.19).

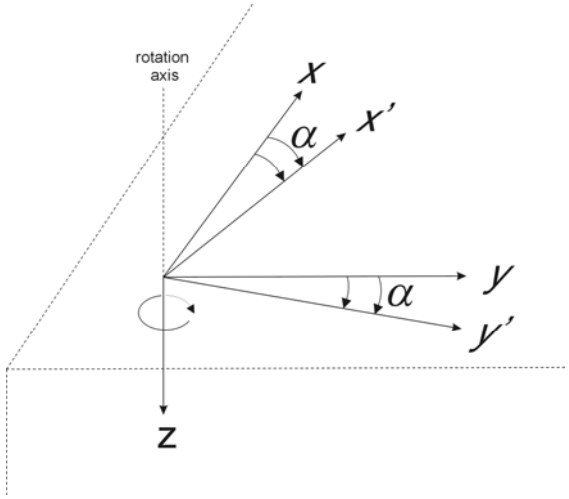

Figure 2.1: Reference frames used to define the magnetotelluric tensor components: xyz are the axes of the original frame. x'y'z are the new axes after a α clockwise rotation, around the z-axis.

For instance, if the rotation is clockwise, the components of $\underline{M}'$ are expressed as:

$$M'_{xx} = M_{xx}\cos^2\alpha + M_{yy}\sin^2\alpha + \left(M_{xy} + M_{yx}\right)\sin\alpha\cos\alpha\,, \tag{2.1a}$$

$$M'_{xy} = \left(-M_{xx} + M_{yy}\right)\sin\alpha\cos\alpha + M_{xy}\cos^2\alpha + M_{yx}\sin^2\alpha\,, \tag{2.1b}$$

$$M'_{yx} = \left(-M_{xx} + M_{yy}\right)\sin\alpha\cos\alpha - M_{xy}\sin^2\alpha + M_{yx}\cos^2\alpha\,, \tag{2.1c}$$

$$M'_{yy} = M_{xx}\sin^2\alpha + M_{yy}\cos^2\alpha - \left(M_{xy} + M_{yx}\right)\sin\alpha\cos\alpha\,. \tag{2.1d}$$

An important rotation-related property of the tensor is its 180^o periodicity:

$$M'_{ij}(\omega)(\alpha + \pi) = M_{ij}(\omega)(\alpha)\,;\ (\text{ij=xx,xy,yx,yy}). \tag{2.2}$$

The rotational properties of the magnetotelluric tensor are those of a 2x2 complex tensor containing eight real and independent variables. Szarka and Menvielle (1997) suggested a set of seven independent real-valued rotational invariants based on three complex magnitudes traditionally used in magnetotellurics:

1) The trace:

$$S_1 = M_{xx} + M_{yy}\,. \tag{2.3a}$$

2) The difference between off-diagonal elements:

$$D_2 = M_{xy} - M_{yx}\,. \tag{2.3b}$$

3) The determinant:

$$\det M = M_{xx}M_{yy} - M_{xy}M_{yx}\,. \tag{2.3c}$$

S_1 and D_2 are two of the four modified impedances (Vozoff, 1991), each one containing two rotational real-valued invariants: Re(S_1), Im(S_1) and Re(D_2), Im(D_2) respectively. From det(M) three independent real-valued invariants can be defined: det(Re(M)), det(Im(M)) and Im(det(M)). This makes a total of seven real and independent rotational invariants.

Other sets of invariants can be defined as a function of these basic invariants. The seven rotational invariants, or just some of them, have been and are still widely used to study particular properties of the MT tensor and other magnitudes related to the measured electromagnetic fields.

2.3 Two-Dimensionality and Strike Direction: Swift's Angle and Skew

As stated in chapter 1, when the measured tensor corresponds to a structure with 2D geoelectric dimensionality, the measuring axes (x, y, z) can be rotated an angle θ (strike angle) such that one of the new axis (x' or y') matches the strike direction of the geoelectric structure. Accordingly, the tensor M' takes a non-diagonal form.

The strike angle can be determined for a perfectly 2D MT tensor by setting equations 2.1a and 2.1d equal to zero. In nature, most 2D MT tensors are not strictly non-diagonal and other strategies are necessary in order to obtain a reliable approximation of the strike direction.

The most common approximation is based on the maximisation of the non-diagonal components of the MT tensor and the minimisation of the diagonal ones, using the sum of the squared modulus of these components (Vozoff, 1972):

$$\left|M'_{xy}(\theta)\right|^2 + \left|M'_{yx}(\theta)\right|^2 = \text{maximum}, \tag{2.4a}$$

$$\left|M'_{xx}(\theta)\right|^2 + \left|M'_{yy}(\theta)\right|^2 = \text{minimum}. \tag{2.4b}$$

The resulting strike angle is known as Swift's angle (Swift, 1967):

$$\tan(4\theta) = \frac{2\cdot\mathrm{Re}(D_1\cdot S_2)}{\left|D_1\right|^2 - \left|S_2\right|^2}, \tag{2.5}$$

where $D_1 = M_{xx} - M_{yy}$ and $S_2 = M_{xy} + M_{yx}$ are the remaining modified impedances (Vozoff, 1991), which are not rotational invariants.

From the modified impedances S_1 and D_2, a rotational invariant, the Swift's skew, can be defined. It relates the diagonal and non-diagonal components of the MT tensor and quantifies how accurately the MT tensor can represent a 2D structure:

$$\kappa = \frac{\left|S_1\right|}{\left|D_2\right|}. \tag{2.6}$$

If its value is small, the 2D hypothesis is valid and, hence, Swift's angle indicates the strike direction. Otherwise, the tensor corresponds to another type of structure.

2.4 Bahr Parameters

Bahr (1991), with modifications of Szarka (1999), proposed the use of four rotational real-valued invariant parameters to classify the types of the geoelectric dimensionality and distortion types that can affect it. These parameters were derived from the impedance tensor ($\underline{Z}=\mu_0\cdot\underline{M}$), and its modified impedances ($S_1=Z_{xx}+Z_{yy}$, $S_2=Z_{xy}+Z_{yx}$, $D_1=Z_{xx}-Z_{yy}$, $D_2=Z_{xy}-Z_{yx}$):

$$\kappa=\frac{|S_1|}{|D_2|}, \text{ (Swift's Skew),} \tag{2.7a}$$

$$\mu=\frac{\left([D_1,S_2]+[S_1,D_2]\right)^{1/2}}{|D_2|}, \tag{2.7b}$$

$$\eta=\frac{\left([D_1,S_2]-[S_1,D_2]\right)^{1/2}}{|D_2|}, \text{ (Regional skew or Phase sensitive skew)} \tag{2.7c}$$

$$\Sigma=\frac{\left(D_1^2+S_2^2\right)}{D_2^2}, \tag{2.7d}$$

where $[A,B]=\mathrm{Re}(A)\cdot\mathrm{Im}(B)-\mathrm{Re}(B)\cdot\mathrm{Im}(A)$.

Bahr parameters are dimensionless. μ and η are normalised to unity whereas κ and Σ can have values greater than one in the presence of galvanic distortion.

κ is the Swift's Skew (see section 2.3) and μ is a measure of the phase difference between the components of the magnetotelluric tensor. η indicates if the magnetotelluric tensor can be described by a superimposition model (the product of a small 3D heterogeneity matrix with the regional 1D or 2D MT tensor, 3D/1D or 3D/2D), which is also a measure of three-dimensionality. Σ is related to two-dimensionality.

The quantification of these parameters, according to Bahr (1991), allows deciphering the geoelectric dimensionality cases (1D, 2D and 3D) and the types of distortion models defined by Larsen (1977) and Bahr (1988). The Larsen (1977) model consists of a galvanic distortion over a 1D structure (3D/1D). The model defined by Bahr (1988), known as superimposition model, consists of a galvanic distortion over a two-dimensional structure: 3D/2D.

The recommended threshold values of these parameters proposed such as to infer the types of geoelectric dimensionality and distortion are summarised in Table 2.1.

In two-dimensional cases (2 and 4) the strike angle, θ, is obtained by the expression:

$$\tan(2\theta)=\frac{[S_1,S_2]-[D_1,D_2]}{[S_1,D_1]+[S_2,D_2]}, \tag{2.8}$$

which is determined from the condition that a 2D MT tensor expressed in the strike reference frame, affected or not by galvanic distortion, has the same phase values in each of the MT tensor columns. This angle is the so-called phase-sensitive strike.

Case	Bahr Parameter Values	DIMENSIONALITY/ DISTORTION TYPE
1	$\kappa < 0.1$; $\Sigma < 0.1$	1D
2	$\kappa < 0.1$; $\Sigma > 0.1$	2D
3	$\kappa > 0.1$; $\mu = 0$	3D/1D (Larsen model)
4	$\kappa > 0.1$; $\mu \neq 0$; $\eta < 0.05$	3D/2D (Bahr model)
5	$\kappa > 0.1$; $\mu \neq 0$; $\eta > 0.3$	3D

Table 2.1: Bahr method criteria to characterise the geoelectric dimensionality and distortion types.

Among these 2D cases, Bahr (1991) also suggested the possibility that the condition cited above is not fulfilled. Instead there is a non-zero phase difference value for each column, which must be minimised when the axes are rotated to the strike direction. This model is known as an extension of the superimposition model, which is called the delta (δ) technique, and is valid under the condition $0.1 < \eta < 0.3$.

In the literature, Bahr parameters have been used sometimes incorrectly, when justifying that the data are 2D if $\eta < 0.3$; whereas it has been demonstrated (e.g. Ledo *et al.*, 2002b) that $\eta > 0.3$ is a sufficient condition for 3D, but that the contrary is not true ($\eta < 0.3$ does not imply that the structure is 2D). Simpson and Bahr (2005) also cite this common misuse of the regional skew η.

2.5 WAL Rotational Invariant Parameters

Weaver *et al*. (2000) presented a new formulation of the rotational invariant parameters of the MT tensor. The set of invariants (WAL hereafter) was redefined in the way that the invariants, with the exception of two, are non-dimensional, each one having a clear graphical representation and their vanishing has a physical interpretation, specifically the geoelectric dimensionality.

The WAL invariants were defined from a decomposition of the MT tensor into its real and imaginary parts, and by defining the complex parameters $\zeta_i = \xi_i + \eta_i i$ (i=1,4), which are

linear combinations of MT tensor components, $\zeta_1 = \left(M_{xx} + M_{yy}\right)/2$, $\zeta_2 = \left(M_{xy} + M_{yx}\right)/2$, $\zeta_3 = \left(M_{xx} - M_{yy}\right)/2$ and $\zeta_4 = \left(M_{xy} - M_{yx}\right)/2$:

$$\underline{M} = \begin{pmatrix} \zeta_1 + \zeta_3 & \zeta_2 + \zeta_4 \\ \zeta_2 - \zeta_4 & \zeta_1 - \zeta_3 \end{pmatrix} = \begin{pmatrix} \xi_1 + \xi_3 & \xi_2 + \xi_4 \\ \xi_2 - \xi_4 & \xi_1 - \xi_3 \end{pmatrix} + i \begin{pmatrix} \eta_1 + \eta_3 & \eta_2 + \eta_4 \\ \eta_2 - \eta_4 & \eta_1 - \eta_3 \end{pmatrix}. \tag{2.9}$$

Through this decomposition, the expressions of the WAL invariants are as follows:

$$I_1 = \left(\xi_1^2 + \xi_4^2\right)^{1/2} \text{ (m/s)}, \tag{2.10}$$

$$I_2 = \left(\eta_1^2 + \eta_4^2\right)^{1/2} \text{ (m/s)}, \tag{2.11}$$

$$I_3 = \frac{\left(\xi_2^2 + \xi_3^2\right)^{1/2}}{I_1}, \tag{2.12}$$

$$I_4 = \frac{\left(\eta_2^2 + \eta_3^2\right)^{1/2}}{I_2}, \tag{2.13}$$

$$I_5 = \frac{\xi_4\eta_1 + \xi_1\eta_4}{I_1 I_2}, \tag{2.14}$$

$$I_6 = \frac{\xi_4\eta_1 - \xi_1\eta_4}{I_1 I_2} = d_{41}, \tag{2.15}$$

$$I_7 = \left(d_{41} - d_{23}\right)/\mathrm{Q}. \tag{2.16}$$

d_{ij} (i,j=1-4) and Q are also invariants that depend on parameters ξ_i η_i and on other invariants:

$$d_{ij} = \frac{\xi_i\eta_j - \xi_j\eta_i}{I_1 I_2}, \tag{2.17}$$

$$\mathrm{Q} = \left[\left(d_{12} - d_{34}\right)^2 + \left(d_{13} + d_{24}\right)^2\right]^{1/2}. \tag{2.18}$$

I_7 and Q are related in that if Q is too small, then I_7 approaches infinity and its value remains undetermined. It can be seen that I_3 to I_6 are normalized and that I_3 to I_7 and Q are dimensionless.

WAL rotational invariants can be represented, following the works of Lilley in a Mohr's circle diagram (Lilley, 1976, 1993, 1998a, 1998b), whose axes display the M_{11} (vertical) and M_{12} (horizontal) components of the MT tensor (Figure 2.2).

In this graphical representation P_1 (Re(M_{11}),Re(M_{12})) and P_2(Im(M_{11}),Im(M_{12})) are the positions of the real and imaginary parts of M_{11} and M_{12} while C and D points are located at coordinates (ξ_1, ξ_4) and (η_1,η_4) respectively. Through a 180º rotation of the measuring axes, P_1 and P_2 describe the complete real and imaginary Mohr circles, with centres located in C and D and radii equal to $(\xi_2^2+\xi_3^2)^{1/2}$ and $(\eta_2^2+\eta_3^2)^{1/2}$ respectively. Hence, a rotation of an angle α is translated into a 2α rotation of points P_1 and P_2.

I_1 and I_2 are the modulae of C and D position vectors, $I_1=|OC|$ and $I_2=|OD|$. I_3 and I_4 are the sines of γ and δ angles, i.e., the ratios between the circles' radii and I_1 or I_2: $I_3=\sin\gamma$ and $I_4=\sin\delta$. $I_5=\sin(\beta+\alpha)$ and $I_6=\sin(\beta-\alpha)$ relate the relative positions between the real and imaginary circles. $2\theta_1$ and $2\theta_2$ are the angles through which P_1 and P_2 must be rotated along the circle to reach the same vertical position as C and D, respectively:

$$\tan(2\theta_1)=-\frac{\xi_3}{\xi_2} \qquad \text{and} \qquad \tan(2\theta_2)=-\frac{\eta_3}{\eta_2}. \tag{2.19}$$

Consequently, θ_1 and θ_2 are, in the order given, the angles through which the measurement axes must be rotated so that the real and imaginary parts belonging to the non-diagonal components of the MT tensor have the same value. I_7 is defined as the sine of the difference between these two angles: $I_7=\sin(\theta_1-\theta_2)$.

Invariant Q is defined from a complex relation between the angle obtained from the intersection of the prolongation of $\overline{CP_1}$ and $\overline{DP_2}$, ψ, and angles α, β, δ and γ: $\mathrm{Q}=\left(\sin^2\gamma+\sin^2\delta-2\sin\gamma\sin\delta\cos(\beta-\alpha-\psi)\right)^{1/2}$.

Invariants I_1 and I_2 provide information about the 1D magnitude and phase of the geoelectric resistivity:

$$\rho_{1D}=\mu_0\frac{\left(I_1^2+I_2^2\right)}{\omega}, \tag{2.20}$$

$$\varphi_{1D}=\arctan\left(\frac{I_2}{I_1}\right). \tag{2.21}$$

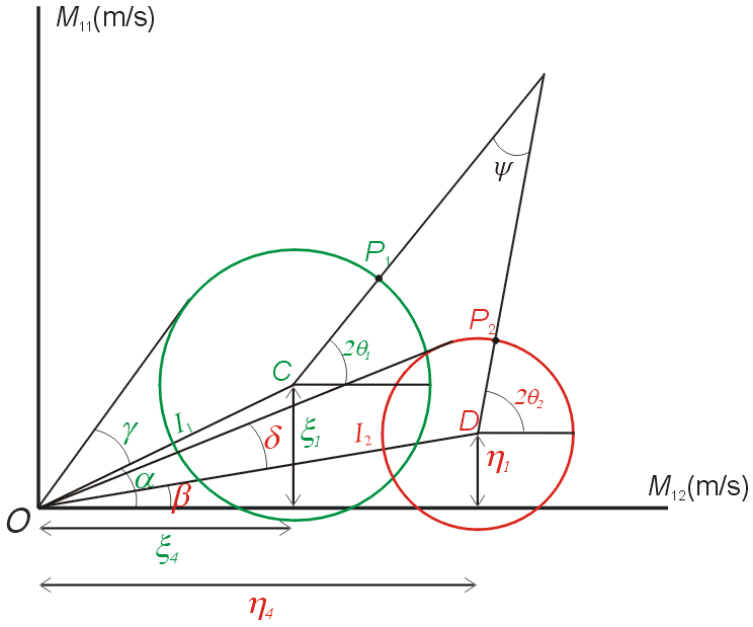

Figure 2.2: Graphical representation of real and imaginary Mohr circles, generated after a complete rotation of M_{12} and M_{11} components of the MT tensor. Green: real circle and related parameters and angles. Red: idem for imaginary.

Invariants I_3 to I_7 and Q make it possible to establish criteria (Weaver *et al.*, 2000; Weaver, pers. comm.) that are suitable to assess dimensionality and galvanic distortion (Table 2.2).

In a 1D geoelectric medium (case 1 in Table 2.2), characterised by a MT tensor with null diagonal components and equal non-diagonal components with opposite signs, the Mohr circles reduce to the two points corresponding to the real and imaginary values of M_{12}. With the exception of I_1 and I_2, all invariants are zero. Apparent resistivity and phase can be directly determined from eqs. 2.20 and 2.21.

For a MT tensor corresponding to a 2D medium (case 2 in Table 2.2), the centres of the Mohr circles are also located over the M_{12} axis, but have non-zero radii values. Along the strike direction, P_1 and P_2 are also located over the M_{12} axis, so both θ_1 and θ_2 are zero. For any other direction, the non-zero values of θ_1 and θ_2 must be the same (equation 2.19), in order to ensure that both real and imaginary diagonal components of the MT tensor become null along the same direction, that of the strike. Since $\overline{CP_1}$ and $\overline{DP_2}$ are parallel the angle ψ is zero. Therefore, in a 2D medium, I_3 and I_4 are non-zero. I_5 and I_6 are null, because α and β angles are null also. I_7 is null, although it may be undetermined if Q is very small (if $I_3 \approx I_4$).

Case	I_3 to I_7 and Q values	GEOELECTRIC DIMENSIONALITY
1	$I_3 = I_4 = I_5 = I_6 = 0$	**1D**
2	$I_3 \neq 0$ or $I_4 \neq 0$; $I_5 = I_6 = 0$; $I_7 = 0$ or Q = 0 ($\xi_4 \neq 0$ and $\eta_4 \neq 0$)	**2D**
3a	$I_3 \neq 0$ or $I_4 \neq 0$; $I_5 \neq 0$; $I_6 = 0$; $I_7 = 0$	**3D/2Dtwist** 2D affected by galvanic distortion (only twist)
3b	$I_3 \neq 0$ or $I_4 \neq 0$; $I_5 \neq 0$; $I_6 = 0$; Q = 0	**3D/1D2D** Galvanic distortion over a 1D or 2D structure (non-recoverable strike direction)
3c	$I_3 \neq 0$ or $I_4 \neq 0$; $I_5 = I_6 = 0$; $I_7 = 0$ or Q = 0 ($\xi_4 = 0$ and $\eta_4 = 0$)	**3D/1D2Ddiag** Galvanic distortion over a 1D or 2D structure resulting in a diagonal MT tensor
4	$I_3 \neq 0$ or $I_4 \neq 0$; $I_5 \neq 0$; $I_6 \neq 0$; $I_7 = 0$	**3D/2D** General case of galvanic distortion over a 2D structure
5	$I_7 \neq 0$	**3D** (affected or not by galvanic distortion)

Table 2.2: Dimensionality criteria according to the WAL invariants values of the magnetotelluric tensor (Modified from Weaver *et al.*, 2000).

Both 1D and 2D media can be affected by galvanic distortion, which, according to WAL invariants, can be grouped into four different cases:

- Galvanic distortion affecting a 2D medium, produced by a twist of the electric field (case 3a in Table 2.2): In this case the galvanic distortion is described by a matrix with parameters $g_1 = g_2$ and $\phi_1 = \phi_2$ ($e = 0$ and $t \neq 0$). In general, the values of M_{11} are not null and the centres of the Mohr circles are not located over the M_{12} axis. $\overline{OC}$ and $\overline{OD}$ have the same orientation, i.e., α and β are non-zero but have the same value. On the contrary, γ and δ are different. θ_1 and θ_2 have the same value ($\overline{CP_1}$ and $\overline{DP_2}$ are parallel), although it does not correspond to the strike direction. Consequently, ψ=0. Hence, I_3, I_4 (where $I_3 \neq I_4$), I_5 and Q are non-zero, whereas I_6 and I_7 are null.

- Galvanic distortion over 1D or 2D media with equal phases in *E* and *B* polarisations (case 3b in Table 2.2): These two situations are indistinguishable, and in the second (distortion over 2D media) it is not possible to determine the strike direction. The Mohr circles follow the same pattern as in case 3a, with the additional particularity that $\gamma=\delta$. Consequently, I_3, I_4 ($I_3 = I_4$) and I_5 are non-zero, and I_6 is null. Given that $I_3 = I_4$ and $\psi=0$, Q is null and I_7 remains undetermined.

- Galvanic distortion over a 1D or 2D medium, resulting in a diagonal MT tensor (case 3c in Table 2.2): This is a very particular case of distortion, described by a non-diagonal matrix. Mohr circles are analogous to those of the 2D media, with the centres located over the M_{11} axis instead of M_{12}, and $\zeta_4 = 0$. WAL invariants can have the same values as in a 2D medium, so case 3c is distinguished from case 3a only by the condition $\zeta_4 = 0$. The strike direction, θ_D, after which the distorted diagonal tensor can be recovered, is computed using:

$$\tan\left(2\theta_D\right)=\frac{\xi_2}{\xi_3}=\frac{\eta_2}{\eta_3}. \tag{2.22}$$

- General case of galvanic distortion over a 2D medium (case 4 in Table 2.2): Mohr circles do not follow any particular pattern (the centres are outside of the M_{12} axis, γ and δ, and α and β are non-zero angles and have different values among them), with the exception that θ_1 and θ_2 have the same value. As a consequence, all invariants but I_7 are non-zero.

For cases 3a and 4, the strike angle, named θ_3, and the distortion parameters, ϕ_1 and ϕ_2 (see equations 1.27 and 1.29) can be retrieved:

$$\tan\left(2\theta_3\right)=\frac{d_{12}-d_{34}}{d_{13}+d_{24}}, \tag{2.23}$$

$$\tan\left(\phi_1\right)=\frac{\mathrm{Re}\,M'_{yy}}{\mathrm{Re}\,M'_{xy}}=\frac{\mathrm{Im}\,M'_{yy}}{\mathrm{Im}\,M'_{xy}}, \tag{2.24}$$

$$\tan\left(\phi_2\right)=\frac{\mathrm{Re}\,M'_{xx}}{\mathrm{Re}\,M'_{yx}}=\frac{\mathrm{Im}\,M'_{xx}}{\mathrm{Im}\,M'_{yx}}. \tag{2.25}$$

Finally, for a MT tensor corresponding to a 3D medium (case 5 in Table 2.2), the pattern of Mohr circles cannot be included in any of the previous descriptions. In this case, all invariants, including I_7 and Q are non-zero and have a finite value. However, it is not possible to distinguish whether the MT tensor is affected by galvanic distortion or not.

The main problem when WAL invariants criteria are used with real data is that the geoelectric dimensionality may be found to be 3D although other evidence (low MT diagonal components' responses, preferred strike direction among different sites and periods…) suggests that a 1D or 2D interpretation would be valid for modelling. This is because invariant values for real data are in general never exactly zero due to the presence of noise. Weaver *et al.* (2000) address this problem by introducing a threshold value, beneath which the invariants are taken to be zero.

The threshold value they suggest is 0.1. Since WAL invariants I_3 to I_7 and Q represent the sines of angles related to Mohr circles, this threshold corresponds to the sine of 5.7^o, which, in relation to 90^o, represents a 6% error. Although the choice of this threshold is subjective, it was tested using a synthetic model with 2% noise, which showed a valid dimensionality pattern consistent with the model structures.

2.6 The Magnetotelluric Phase Tensor

The magnetotelluric phase tensor (or phase tensor) (Caldwell *et al.*, 2004) was introduced as a tool to obtain information about the dimensionality of the regional structure, given that it is not affected by galvanic distortion.

The phase of a tensor with complex components is a real valued tensor, Φ, which is defined from the generalization of the phase of a complex number, i.e., as the inverse of the tangent of the ratio between its imaginary and real parts (Caldwell *et al.*, 2004):

Thus, for a complex tensor $\underline{M}=X+i\cdot Y$:

$$\Phi = X^{-1}Y\ . \tag{2.26}$$

In the case of the magnetotelluric or impedance tensor, which is a 2nd rank tensor,

$$\underline{M} = \begin{bmatrix} X_{11}+iY_{11} & X_{12}+iY_{12} \\ X_{21}+iY_{21} & X_{22}+iY_{22} \end{bmatrix}, \tag{2.27}$$

the phase tensor (Φ) is expressed as:

$$\Phi = \begin{bmatrix} \Phi_{11} & \Phi_{12} \\ \Phi_{21} & \Phi_{22} \end{bmatrix} = \begin{bmatrix} X_{22}Y_{11} - X_{12}Y_{21} & X_{22}Y_{12} - X_{12}Y_{22} \\ X_{11}Y_{21} - X_{21}Y_{11} & X_{11}Y_{22} - X_{21}Y_{12} \end{bmatrix} / \det(X), \quad (2.28)$$

where $\det(X) = X_{11}X_{22} - X_{12}X_{21}$.

Φ is not affected by galvanic distortion, although it is not invariant under rotation.

In the particular 1D case, the phase tensor takes a diagonal form, with their two component values equal to the tangent of the phase (equations 1.15c and 1.15d). As for a 2D MT tensor, the phase tensor is also diagonal, but their components have different values, which are the tangents of the TE and TM phases. In a general 3D case, the phase tensor displays the relationship between the phases of the horizontal components of the electric and magnetic fields.

The phase tensor can be represented through a Singular Value Decomposition (SVD) as the product of three matrixes:

$$\Phi = R^T(\alpha_P - \beta_P) \cdot S \cdot R(\alpha_P + \beta_P) = R^T(\alpha_P - \beta_P) \begin{bmatrix} \Phi_{Max} & 0 \\ 0 & \Phi_{min} \end{bmatrix} R(\alpha_P + \beta_P), \quad (2.29)$$

where R(δ) ($\delta = \alpha_P$ - β_P or $\delta = \alpha_P + \beta_P$) represents a clockwise rotation,

$$R(\delta) = \begin{bmatrix} \cos\delta & \sin\delta \\ -\sin\delta & \cos\delta \end{bmatrix}. \quad (2.30)$$

$R^T(\alpha_P$ - $\beta_P)$ and $R(\alpha_P + \beta_P)$ are the eigenvectors of the tensor products $\Phi^T\Phi$ and $\Phi\Phi^T$ respectively. The expressions of α_P and β_P are derived as [1]:

$$\alpha_P = \arctan\left(\frac{\Phi_{12} + \Phi_{21}}{\Phi_{11} - \Phi_{22}}\right) / 2, \quad (2.31)$$

$$\beta_P = \arctan\left(\frac{\Phi_{12} - \Phi_{21}}{\Phi_{11} + \Phi_{22}}\right) / 2. \quad (2.32)$$

S in eq. 2.29 is referred to as the Singular Matrix, where Φ_{Max} and Φ_{min} are the square roots of $\Phi^T\Phi$ or $\Phi\Phi^T$ eigenvalues, real numbers which are arranged in descending order in S:

[1] The original notation of Caldwell *et al.* (2004) used the notation α and β instead of α_P and β_P. In this thesis the subscript "***P***" was added to emphasize that it refers to the magnetotelluric **p**hase tensor notation.

$$\Phi^2_{\substack{Max\\min}} = \frac{Tr(\Phi\Phi^T) \pm \sqrt{Tr(\Phi\Phi^T)^2 - 4\det(\Phi\Phi^T)}}{2}. \qquad (2.33)$$

Since Φ is a 4 real component tensor, it has 4 associated parameters: One, the angle α_p, which is not a rotational invariant, and three rotational invariants: β_P, Φ_{Max} and Φ_{min} (eq. 2.29).

β_P is the skew of the phase tensor. In a two-dimensional medium its value is zero.

Simpler expressions of Φ_{Max} and Φ_{min} in terms of the phase tensor components can only be obtained for 1D and 2D geoelectric media. These expressions are the tangents of regional TE and TM mode phases, and, depending on which has the maximum and minimum values could be:

$$\Phi_{\substack{Max\\min}} = \tan\varphi_{\substack{TE\\TM}} \qquad \text{or} \qquad \Phi_{\substack{Max\\min}} = \tan\varphi_{\substack{TM\\TE}}. \qquad (2.34)$$

Hence, each of these parameters is related to one of the two directions along which a linear polarization of the magnetic field leads to a linear polarization of the electric field. If Φ_{Max} and Φ_{min} have the same value, there is not a preferential direction and the structure is 1D, whereas if Φ_{Max} and Φ_{min} are different, these two directions exist and indicate that the structure is 2D, as long as β_P=0. For general 3D cases, Φ_{Max} and Φ_{min} are also different and $\beta_P \neq 0$, resulting in more complex expressions. In real datasets, the threshold of β_P to identify 3D cases is approximately 3°.

The phase tensor can be represented as an ellipse in which Φ_{Max} and Φ_{min} are the major and minor axis and α_P - β_P is the azimuth of the major axis (Figure 2.3). In the case that β_P=0, this azimuth coincides with α_P and represents the strike direction or its perpendicular, depending on which TE or TM modes has the largest phase value.

The way in which α_P, Φ_{Max} and Φ_{min} are related is that α_P has a physical meaning only if $|\Phi_{Max} - \Phi_{min}|$ is non-zero, i.e., in 2D and 3D cases. If data errors are considered, this assertion can be extended to the condition $\arctan|\Phi_{Max} - \Phi_{min}| > \sigma_{\alpha_P}$, where σ_{α_P} is the error in the determination of angle α_P.

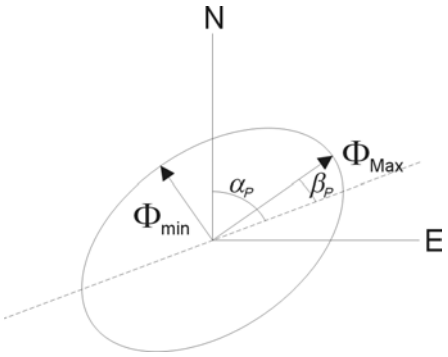

Figure 2.3: Graphical representation of the phase tensor. The lengths of the principal axes are Φ_{Max} and Φ_{min} and α_P - β_P is the azimuth of the ellipse major axis. N and E correspond to x and y coordinates axes respectively (Modified from Caldwell *et al.*, 2004).

Figure 2.4 shows the phase tensor characteristics and representation for 1D and 2D types of dimensionality: 1D media are represented by a circle, given that $\left|\Phi_{Max} - \Phi_{min}\right|$ is equal to zero and α_P has a meaningless value. 2D media are represented by an ellipse with the major axis aligned along the strike direction, α_P. For 3D geoelectrical media, the phase tensor is displayed as in Figure 2.3: an ellipse with β_P different from zero and consequently with an angle α_P that cannot be identified as the strike direction.

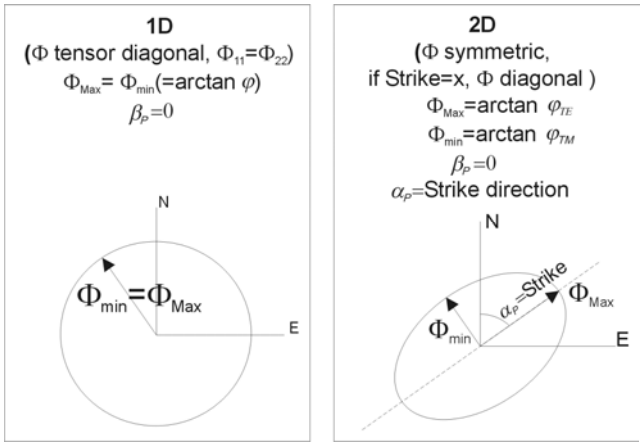

Figure 2.4: Phase tensor properties and representations of particular 1D and 2D dimensionality cases.

Summarizing, the phase tensor parameters involved in the characterization of dimensionality are: Φ_{Max} and Φ_{min}, which provide the arctangent of TE and TM mode phases;

their difference, $\left|\Phi_{Max}-\Phi_{min}\right|$, which indicates if the structure can be described as 2D; β_P, which quantifies the validity of a 2D description, and α_P, which provides the strike direction. In 2D media, the error of angle α_P is also important since, compared to $\left|\Phi_{Max}-\Phi_{min}\right|$, it allows discerning whether a 2D or 3D/2D description is valid or not.

Since the phase tensor is not affected by galvanic distortion, it preserves information of the regional structures. In this way, maps of the elliptical diagrams of the phase tensor at a given frequency reflect lateral variations of the regional structures, in which the major axes of the ellipses, Φ_{Max}, indicate the direction of the induced current flow (e.g. Caldwell *et al.*, 2004).

2.7 Problems and Present Limitations on the Determination of Dimensionality

As already seen, the determination of geoelectric dimensionality is not a simple nor easy task. It is a problem that must be solved through the use of methods such as Bahr and WAL parameters and the more recent phase tensor. All these methods, although allowing dimensionality characterisation, have some limitations, which make it difficult to solve the problem in many cases.

Firstly, the determination of geoelectric dimensionality corresponding to MT data utilise parameters that are affected by the errors in the data responses. It is important to take into account the errors of these parameters in the determination of dimensionality and to know to which degree the feasibility of the characterised structures is.

Another important aspect to consider is the fact that in real situations, the dimensionality of the data does not fit exactly to the theoretical models described. A compromise between both descriptions can be achieved by using threshold values in the dimensionality criteria.

However, the parameters used in the presented methods and the choice of the threshold values imply that the dimensionality is not characterised in the same way. Sometimes they provide inconsistent results or different types of information, which can lead to incorrect hypotheses in modelling and interpretation of the data.

In this context, the next part of the thesis presents the studies, comparisons and new developments carried out on the characterisation of geoelectric dimensionality. These propose solutions to partially or totally solve some of these problems and limitations. More specifically, these aspects are: Error analysis and threshold values in WAL rotational invariants (Chapter 3), Improving Bahr's invariant parameters using the WAL approach (Chapter 4) and Applications of the magnetotelluric phase tensor and comparison with other methods (Chapter 5).